



Power Electronic Systems
Laboratory

© 2012 IEEE

Proceedings of the 38th Annual Conference of the IEEE Industrial Electronics Society (IECON 2012), Montreal, Canada,
October 25-28, 2012

Soft-Switching Techniques for Medium-Voltage Isolated Bidirectional DC/DC Converters in Solid State Transformers

G. Ortiz,
D. Bortis,
J. W. Kolar,
O. Apeldoorn

This material is published in order to provide access to research results of the Power Electronic Systems Laboratory / D-ITET / ETH Zurich. Internal or personal use of this material is permitted. However, permission to reprint/republish this material for advertising or promotional purposes or for creating new collective works for resale or redistribution must be obtained from the copyright holder. By choosing to view this document, you agree to all provisions of the copyright laws protecting it.



Eidgenössische Technische Hochschule Zürich
Swiss Federal Institute of Technology Zurich

Soft-Switching Techniques for Medium-Voltage Isolated Bidirectional DC/DC Converters in Solid State Transformers

G. Ortiz*, D. Bortis*, J. W. Kolar*, O. Apeldoorn**

*Power Electronic Systems Laboratory, ETH Zurich

**Power Electronics and Medium Voltage Drives, ABB Switzerland AG

Email: ortiz@lem.ee.ethz.ch

Abstract—Soft switching techniques are very attractive and often mandatory requirements in medium-voltage and medium-frequency applications such as solid state transformers. The effectiveness of these soft switching techniques is tightly related to the dynamic behavior of the internal stored charge in the utilized semiconductor devices. For this reason, this paper analyzes the behavior of the internal charge dynamics in high-voltage semiconductors, giving a clear base to understand the previously proposed zero-current-switching techniques for IGBT-based resonant dual-active-bridges. From these previous approaches, the two main concepts that allow switching loss reduction in high-voltage semiconductors are identified: 1) shaping of the conducted current in order to achieve a high recombination time in the previously conducting semiconductors and 2) achieving ZVS in the turning-on device. The means to implement these techniques in a triangular current mode dual-active-bridge converter together with the benefits of the proposed approaches are analyzed and experimentally verified with a 1.7 kV IGBT-based NPC bridge. Additionally, the impact of the modified currents in the converter's performance are quantified in order to determine the benefits of the introduced concepts in the overall converter.

I. INTRODUCTION

Transformers operating in line frequency (50/60Hz) are key components within today's electric power systems as they provide the link between grids with different voltage levels, namely high-voltage, medium voltage (MV) and low voltage (LV) grids. These transformers however, are characterized by several limitations such as large size/weight, ideally equal input and output active and reactive power, equal input and output operating frequency and tightly linked input and output voltages.

These limitations can be overcome by building a transformer based on power electronic devices, i.e. a Solid State Transformer (SST). An example of a single-phase SST is shown in Fig. 1-a). Here, the medium-voltage side AC/AC converter is used to actively shape the input current i_{MV} , for example, to reach a unity power factor or in other cases, if a capacitive buffer is provided inside the AC/AC converter, to act as an active filter and/or a static Var compensator. The link between the MV and the LV AC/AC converters is done through a transformer whose operating frequency f_{MF} lies in the Medium Frequency (MF) range, thus achieving a small size/weight and a faster dynamic response. On the LV side, the characteristics of the output AC voltage, namely amplitude u_{LV} and frequency f_{LV} , can be actively controlled with little dependency on the medium voltage side voltage u_{MV} and frequency f_{MV} . These additional functionalities are envisioned as the key enabling features for future compact traction solutions [1, 2], grid integration of renewable energy generation [3–5] and smart grid implementation [6, 7], among others.

One possible structure for the SST is a three-stage concept [6] presented in Fig. 1-b). In this concept, AC/DC MV and LV converters are connected to the MV and LV AC grids respectively. The DC-links of these AC/DC converters are linked through a high power DC/DC converter, where the isolation and voltage

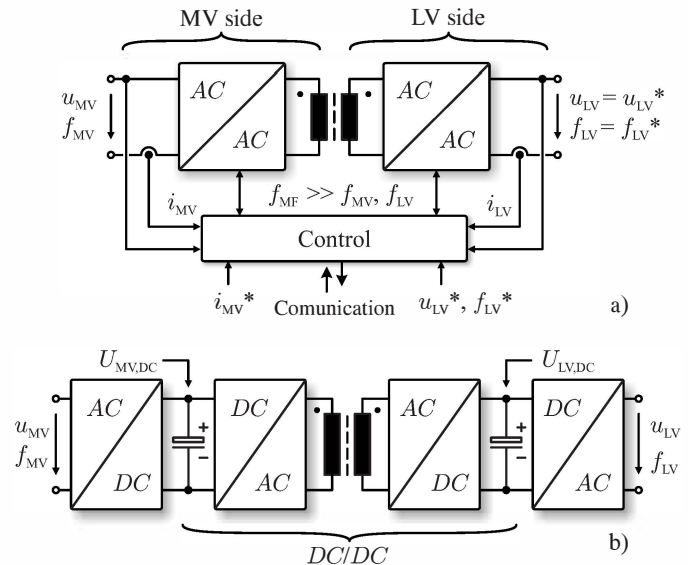


Figure 1: Solid state transformer: a) Single phase structure; b) Three-stage concept comprising high-power DC/DC converter.

step-down is provided through a MF AC-link. In the DC/DC converter, the semiconductors in the MV side bridge are required to block voltages in the kilovolt range, therefore IGBTs are a very attractive choice. These semiconductors however, are characterized by a bipolar power stage which, in order to block these high voltages, comprises a considerably large n^- drift region which stores a large amount of charge during the conduction phase of the

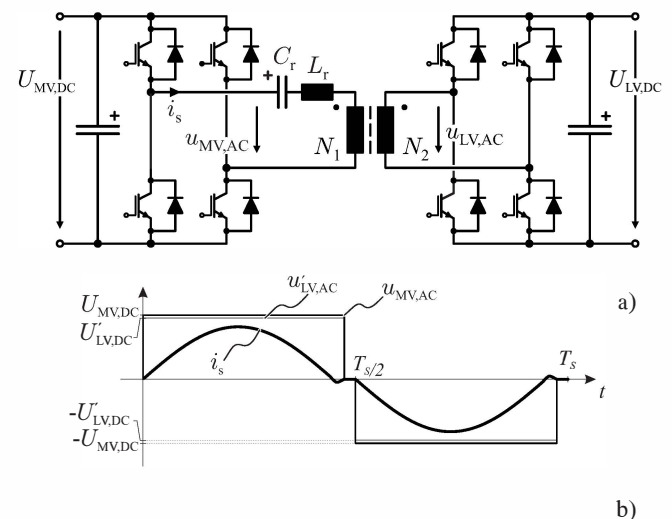


Figure 2: Series resonant DAB: a) Power circuit linking MV to LV DC buses; b) Voltage and current in the AC link.

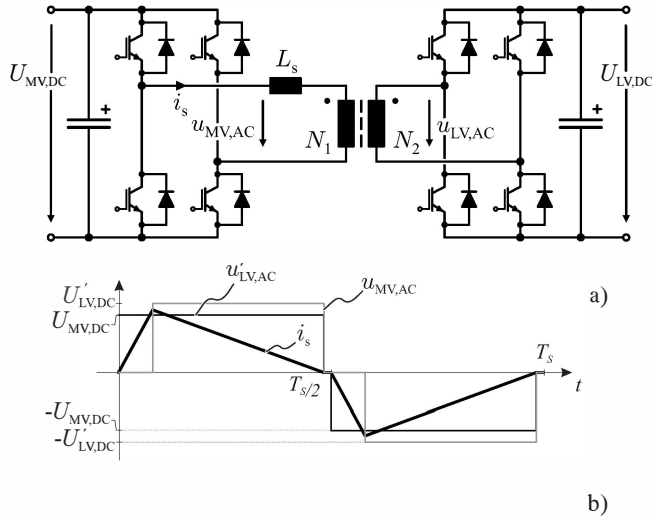


Figure 3: Triangular current DAB: a) Power circuit linking MV to LV DC buses; b) Voltage and current in the AC link.

semiconductor. When the switch is turned-off, this stored charge is evacuated from the semiconductor, causing tail currents which overlap with the blocking voltage, hence generating high switching losses. If operated in the MF range, these switching losses would be unbearable, unless the current through the semiconductors is conveniently shaped during its conduction phase in order to achieve Zero-Current-Switching (ZCS).

A widespread topology that can allow bidirectional power flow and ZCS operation, investigated mainly in traction applications, is the series resonant Dual Active Bridge (DAB) converter [1, 8–12] (cf. Fig. 2). This topology consists of two active bridges linked through a MF transformer in series with a resonant tank. When operated below resonant frequency, this converter allows the MV and LV side switches to operate in ZCS, thus reducing their switching losses. Nevertheless, these switching losses are not negligible in spite ZCS operation. For this reason, several enhancements to the ZCS modulation scheme that allow a further reduction in the switching losses have been previously reported, whereby the main approaches are revised in this paper.

The main disadvantage of the series resonant DAB, besides its lower power density and high current requirement of the series resonant capacitor C_r , is its incapability to control the transferred power while still achieving ZCS. In case power transfer control is required, the Triangular Current Mode (TCM) DAB presents an attractive solution [13] (cf. Fig. 3). In this converter, the resonant tank is replaced by a series inductor L_s . By properly selecting the transformer turns ratio, the MV side switches can be operated in ZCS mode in both power directions while actively controlling the transferred power by adjusting the LV side duty cycle [14, 15]. In this case however, ZCS on the LV side is not possible.

In this paper, an initial analysis on the stored charge dynamics in high-voltage semiconductor devices is performed in **Section II**, which gives the base to study in **Section III** the previously proposed ZCS methods in series resonant DABs. With this revision, novel concepts for switching-loss reduction in the TCM DAB converter by means of soft switching techniques are proposed and experimentally validated in **Section IV**. The reduction in switching losses in the MV side of the TCM DAB results in modified current shapes in the converter, therefore the impact of these new current shapes in the overall converter performance is quantitatively studied at the end of **Section IV**.

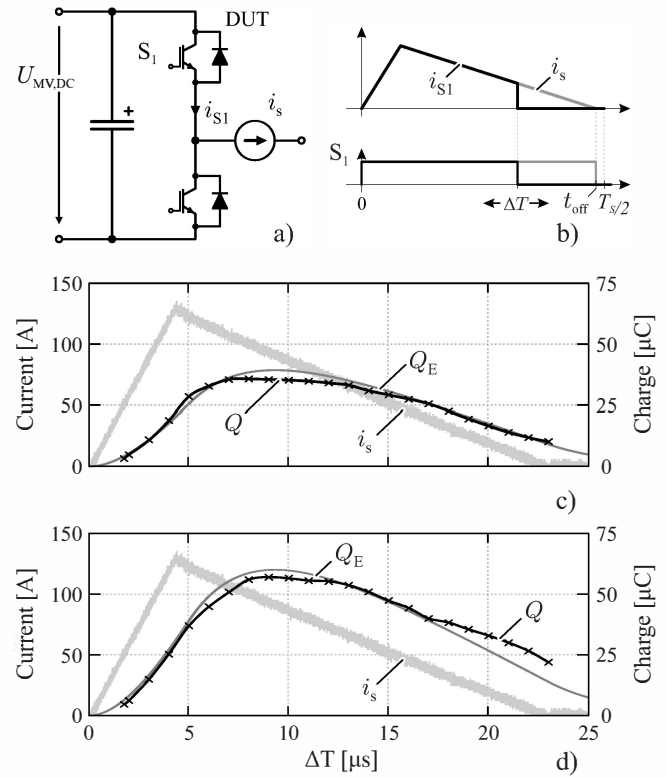


Figure 4: In order to measure the semiconductor's stored charge, the circuit in a) was used. The triangular current shape shown in b) is generated by the current source i_s in a) and is used to measure stored charge in 1.7 kV IGBTs for c) 25 °C and d) 120 °C junction temperature.

II. SEMICONDUCTOR STORED CHARGE DYNAMICS

High voltage bipolar semiconductor devices, as previously mentioned, store large amounts of charge during their conduction phases. This charge, if not allowed to recombine internally, is translated into switching losses when the device is taken back to the blocking state. Since this stored charge is directly related to the dissipated energy during the switching process, it is useful to analyze the behavior of the charge Q stored in the switch during its conduction phase.

Consider the circuit depicted in Fig. 4-a) where an IGBT-based bridge leg is presented. Here, a current source generates the triangular current i_s shown in Fig. 3-b) whereby switch S_1 is turned on at $t = 0$, the beginning of the switching period, and turned-off at $t = \Delta T$. By increasing stepwise the value of ΔT from $\Delta T = 0$ to $\Delta T = t_{\text{off}}$, the current turned-off by device S_1 is modified, as shown in Fig. 4-b). Measuring the current i_{s1} through S_1 and integrating it during the switching process for each value of ΔT , the charge stored in the device during the conduction phase can be constructed.

This experiment was performed on a bridge leg based on 1.7 kV PT IGBTs (FF150R17KE4) operating at 20 kHz with a DC-link voltage of $U_{\text{MV,DC}} = 1$ kV and reaching a peak current of 140 A. The results for the behavior of the charge Q for junction temperatures of 25 °C and 120 °C are presented in Figs. 4-c) and d) respectively.

From Fig. 4-c) it can be seen that the stored charge Q is not proportional to the conducted current, therefore it can be already concluded that switching losses under these conditions do not depend on the instantaneous value of the switched current. This

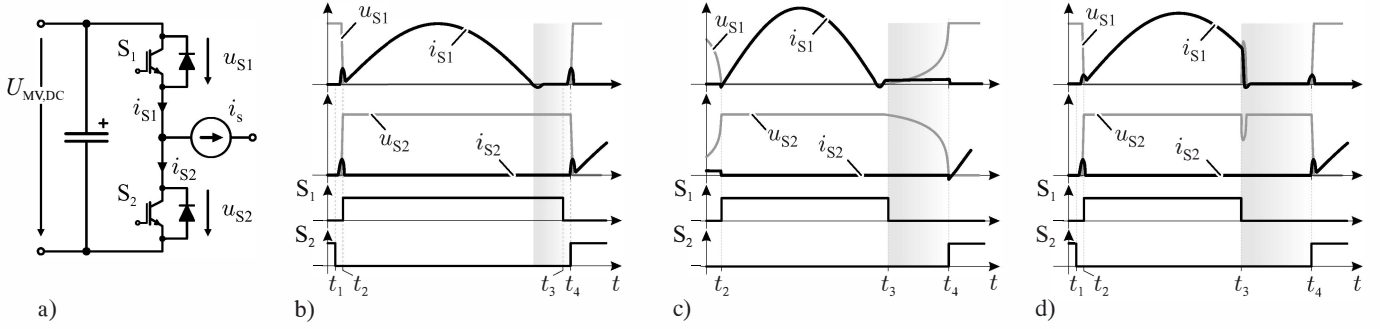


Figure 5: Previously reported enhancements to the ZCS resonant DAB: a) IGBT phase leg; b) Interlock time introduced; c) Increased magnetizing current; d) Non ZCS.

TABLE I: Extracted parameters for the 1.7 kV PT IGBT at junction temperatures of $T_j = 25^\circ\text{C}$ and $T_j = 120^\circ\text{C}$

Parameter	$T_j = 25^\circ\text{C}$	$T_j = 120^\circ\text{C}$
τ_r	3.2 μs	3.3 μs
k_r	0.1	0.18

means, for example, that by switching the peak current of 140 A at $t = 4 \mu\text{s}$, less charge is removed, hence lower switching losses are generated, in comparison to switching at $t = 10 \mu\text{s}$, when the value of the switched current is considerably lower. Moreover, at time $t = 22 \mu\text{s}$ when the current reaches zero, a considerable amount of charge remains stored in the device, thus turning S_1 off in ZCS conditions wouldn't result in zero switching losses. The results with junction temperature of 120°C (cf. Fig. 4-d)) show a similar behavior whereby the total value of stored charge during the whole conduction phase is higher in comparison to operation at 25°C , therefore the zero-current switching losses would be also increased. This analysis was also performed in [16] for a resonant structure, where the dynamic behavior of the internal semiconductor charge was also observed.

In order to complete the analysis, the charge control equation, described in [17], is used to find a simple analytical expression that estimates the behavior of the internal charge $Q(t)$ in the semiconductor during its conduction phase:

$$\frac{dQ(t)}{dt} + \frac{Q(t)}{\tau_r} = k_r \cdot i_s(t), \quad (1)$$

where τ_r is the recombination time constant, $i_s(t)$ is the current through the device during its conduction phase and k_r is a current proportionality parameter tightly related to the IGBT construction and the operating junction temperature T_j .

Solving (1) for $Q(t)$ with the current i_s shown in Fig. 4-b) and performing curve fitting results in the values of τ_r and k_r shown in Table I. With these parameters, the estimated charge behavior Q_E is calculated and plotted in Figs. 4-c) and d) for the respective operating temperatures. As can be seen, a good agreement with respect to the experimental values of stored charge is achieved, therefore the charge control equation (1) proves useful to estimate the behavior of the stored charge in this type of IGBTs. This means that, provided that IGBT manufacturers include information about the recombination time constant τ_r and the proportionality constant k_r in the device's datasheet, a better estimation of the switching losses for an arbitrary current shape can be achieved. The precise relation of the charge behavior and the respective losses will be matter of study for future publications.

Based on the previous stored charge analysis, the first observation regarding soft switching techniques in high voltage semiconductors can be made: the shape of the current during the conduction

phase highly influences the remaining stored charge that needs to be evacuated from the switch when entering the blocking state. Therefore, it is desirable to conveniently shape this current in order to minimize the ZCS losses, as reported in previous publications on the series resonant DAB (cf. Fig. 2) whereby the main approaches are revised in the next section.

III. PREVIOUSLY PROPOSED ZCS TECHNIQUES IN RESONANT CONVERTERS

Consider the bridge leg presented in Fig. 5-a) where the current source i_s represents the resonant tank together with the rest of the series resonant DAB circuit (cf. Fig. 2-a)). This current source generates the sinusoidal pulses shown in Figs. 5-b), c) and d) used to analyze three of the main previously proposed enhancements in the ZCS modulation scheme for this converter structure: *A. Interlock Time*; *B. Increased Magnetizing Current* and *C. Giving up ZCS*.

A. Interlock Time

As described in [8, 18], the resonant converter offers the possibility to introduce an interlock time in the conduction of S_1 between the zero crossing of the current and the turn-on event of S_2 , as seen in Fig. 5-b). This interlock time provides additional time for the IGBT to recombine its carriers in a lossless manner, thus the switching losses generated when S_2 is turned on are considerably reduced.

B. Increase in Magnetizing Current

In the series resonant DAB converter, the bridge providing the power also needs to provide the magnetization current for the isolation transformer. This means that when the resonant pulse is finished, the magnetizing current continues flowing through the previously conducting IGBTs, as shown in Fig. 5-c). Therefore, if the magnetizing current is made high enough, it can be used to extract stored charge from the IGBT, as described in [11, 18]. It should be noted that, if enough time is provided to change the voltage in S_1 and S_2 , the turn on process of S_2 is done under ZVS conditions, thus a great reduction in switching losses can be achieved.

C. Giving up ZCS

As reported in [8, 18], switch S_1 in Fig. 5-a) can be turned off before the resonant pulse has reached zero current. This way, the charges stored in the IGBT can be removed by the resonant inductor and, under certain conditions, ZVS can be achieved in the turning-on IGBT. In order to achieve this, the resonant inductor L_r must store enough energy to charge/discharge S_1 and S_2 .

A large resonant inductor, however, is undesirable in this converter since it affects its dynamic performance and it can cause

problems related to the reverse recovery of the rectifying diodes. For this reason, turning-off S_1 , as shown in Fig. 5-d), does not result in a traditional inductive switching. Nevertheless, this type of switching strategy has reported reduction in switching losses in previous implementations [8, 18] due to the additional time that can be provided for carrier recombination (shaded area in Fig. 5-d)).

D. Applications to the TCM DAB converter

The aforementioned enhancements to the ZCS modulation in the series resonant DAB suggest the use of similar techniques in the TCM DAB. In case of the additional interlock time, its implementation in the TCM DAB is not straightforward. This is due to the reverse recovery of the rectifying diodes in the LV side. In the resonant converter, the series inductor L_r is typically kept as low as possible to improve the converter dynamic response. This results in a large resonant capacitor C_r value, thus the peak voltage in this component is low in comparison to the DC-link voltages. The peak resonant capacitor voltage must be blocked by the diodes in the rectifying bridge after their respective conduction phases, therefore, since this voltage step is considerably low, the reverse recovery effects are negligible, as reported in [8, 11, 18].

On the other hand, in the TCM DAB, this voltage step is considerably larger as it corresponds to the MV side applied voltage times the turns ratio of the transformer, resulting in large oscillations in the AC link voltages due to the reverse recovery of the rectifying diodes. Therefore, other strategies to provide longer recombination time need to be implemented in the case of the TCM DAB.

Since the value of the series inductor L_s in case of the TCM DAB is considerably higher than its resonant counterpart L_r , the stored energy in this component is considerably higher. This means that, by properly adjusting the control signals in the TCM DAB, the switches can perform switching of current, thus giving up ZCS, with high enough value to completely remove the stored charge in the devices while achieving ZVS in the complementary switch. This can be achieved without reducing the magnetizing inductance value, as in the series resonant DAB, and therefore without increasing the reactive power in the circuit. The modification to the modulation scheme that allows this behavior is introduced and experimentally verified in the next section.

IV. PROPOSED ENHANCEMENTS TO THE TCM DAB

As discussed in the previous sections, there are two main strategies that can help to reduce switching losses in HV semiconductors. The first one is related to the time provided for the recombination of the charge that the device stores during its conduction phase by introducing a time interval before the semiconductor blocks when the current is considerably lower than the peak current. The second one is the reduction or total elimination of turn-on losses by achieving ZVS in the turning-on device. This can be achieved by turning off a current (giving-up ZCS) through a modification in the modulation scheme in the TCM DAB. The means to implement these strategies will be discussed in this section together with their experimental verification.

A. Standard ZCS Modulation

In order to benchmark the proposed modulation strategies for the TCM DAB, first the switching losses in the standard ZCS modulation scheme studied in [13–15] were measured. These measurements were performed with 1.7 kV IGBTs (FF150R17KE4) which are based on field-stop technology. Because of its similarity to a punch-through IGBT, this technology is well suited for ZCS applications due to its short recombination time [16, 17]. These

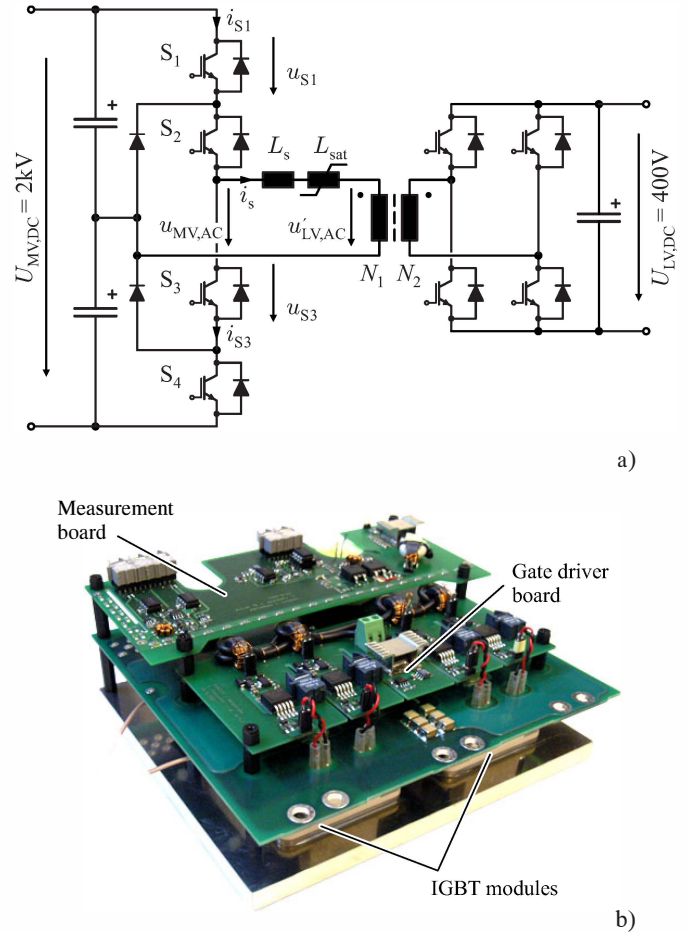


Figure 6: DAB converter used to test the 1.7 kV PT IGBTs: a) NPC-based bridge linked to the LV full-bridge through a $N_1/N_2 = 3/1$ transformer; b) Hardware realization of the MV side NPC 2kV bridge.

1.7 kV IGBTs build a 2 kV NPC-based bridge as shown in Fig. 6-a) designed for nominal power of 166 kW and 20 kHz of switching frequency. The hardware realization of this bridge is shown in Fig. 6-b). The non-linear inductor L_{sat} shown in Fig. 6-a) will be used in the third part of this section to shape the current in order to reduce the switching losses in the MV side switches. The transformer turns ratio is $N_1/N_2 = 3/1$ and the LV side bridge is a 400 V full-bridge structure utilized to generate the desired current waveforms. Planar current transformers and passive voltage probes were used to measure the currents and voltages respectively in switches S_1 , S_2 , S_3 and S_4 (cf. Fig. 6-a)).

The operation of the bridge shown in Fig. 6 (without the saturable inductor L_{sat}) under ZCS was performed, as shown in Figs. 7 and 8. In Fig. 7-a) the operation during the positive semi cycle for power transfer from MV to LV is shown. The cycle starts with zero current through inductor L_s and the MV bridge applying positive voltage on its output while the LV side stays in freewheeling mode, thus half of the MV side DC voltage is applied to inductor L_s causing a linearly increasing current. When the peak current is reached around $t = 5 \mu s$, the LV side is switched and applies the LV DC voltage on its output, thus the difference between the MV side DC voltage and the reflected LV side DC voltage is applied to the series inductor L_s . Due to the transformer's turns ratio $N_1/N_2 = 3/1$, this causes a voltage of $-200 V$ applied to the inductor L_s , hence the current decreases linearly. As soon as the current reaches zero,

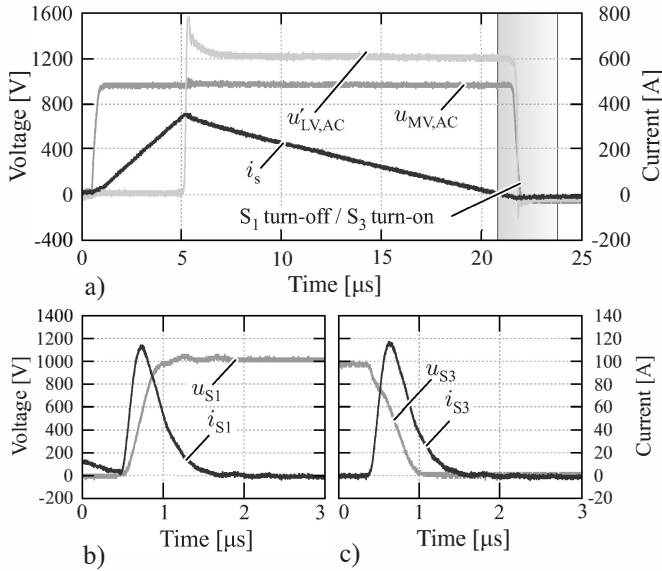


Figure 7: Main waveforms in standard ZCS with TCM DAB and power from MV side to LV side: a) AC-link waveforms for half switching period; b) Voltage and current in S_1 during the time instant highlighted in a); c) Voltage and current in S_3 during the time instant highlighted in a).

both the MV and LV side bridges are switched to freewheeling, thus applying zero voltage on their outputs while achieving ZCS. The turn-off and turn-on process of complementary switches S_1 and S_3 respectively are used herein in order to exemplify the ZCS process and the further enhancements. It should be noted however that for a comprehensive switching loss analysis, all switching events were measured and used to calculate the total losses in the NPC bridge.

The switching process of devices S_1 and S_3 during the highlighted time interval in Fig. 7-a) is shown in Figs. 7-b) and c) respectively. Here it can be seen that, since S_1 was conducting the current during the positive semi cycle, it contains a considerable amount of stored charge, which is removed when S_3 is turned on causing turn-off losses in S_1 as well as considerable turn-on losses in S_3 .

The current and voltage waveforms in the transformer for power flowing from LV to MV are shown in Fig. 8-a), where the phase shift and duty cycles of the LV and MV side bridges have been adjusted to achieve the power flow in the reverse direction while still achieving ZCS in the MV side. The switching behavior of switches S_1 and S_3 is shown in Figs. 8-b) and c) respectively where it should be noted that for this power direction the respective antiparallel diodes of each switch conduct the triangular current and are therefore responsible for the generated switching losses. As can be seen, the turn-on process of S_3 generates losses in the antiparallel diode of S_1 , as this last device was previously conducting the full current thus it contains considerable amount of stored charge. The current peak in Figs. 8-b) and c) representing the evacuation of charge stored in the antiparallel diode of S_1 flows through S_3 during its turn-on process, thus causing turn-on losses also in this last device (cf. Fig. 8-c)).

The waveforms shown in Figs. 7 and 8 suggest the use of a modified modulation scheme where a certain amount of current is switched-off by S_1 . This way, the stored charge accumulated during its conduction phase is evacuated through the load, thus decreasing the voltage of S_3 before its gate signal is applied, thus achieving ZVS in this last device and ideally a lossless commutation.

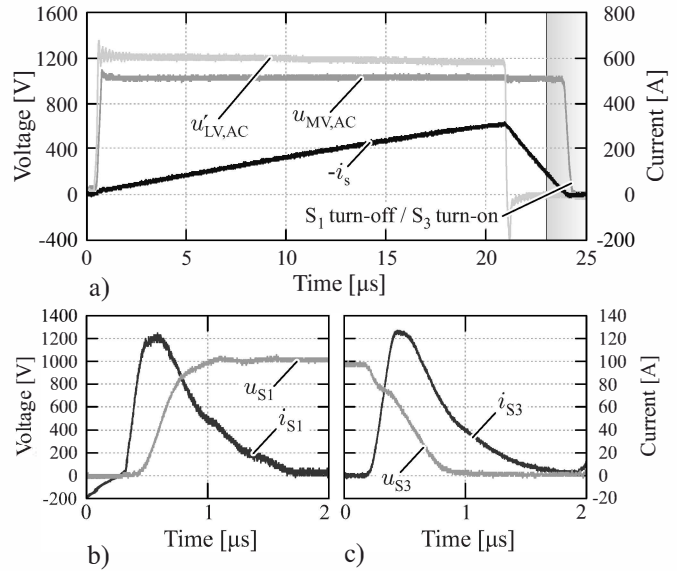


Figure 8: Main waveforms in standard ZCS with TCM DAB and power from LV side to MV side: a) AC-link waveforms for half switching period; b) Voltage and currents in S_1 during the time instant highlighted in a); c) Voltage and current in S_3 during the time instant highlighted in a).

B. Modified ZVS Modulation

The operation under ZVS was studied for the converter displayed in Fig. 6 (without the saturable inductor L_{sat}). The waveforms for power from MV to LV are shown in Fig. 9-a), where the duty cycles and phase shift are adjusted in order to achieve ZVS in the MV side bridge. In this case, S_1 is turned-off before the current reaches zero, thus loosing ZCS, as shown in Fig. 9-b). Since the current is not zero when S_1 is turned off, its voltage increases before the gate signal is applied to its complementary switch S_3 . This means that S_3 is turned on with ZVS and no current peak must be conducted during its turn-on process (cf. Fig. 9-c)), in contrast to the switching process shown in Fig. 7-c), thus reducing the turn-on losses in S_3 .

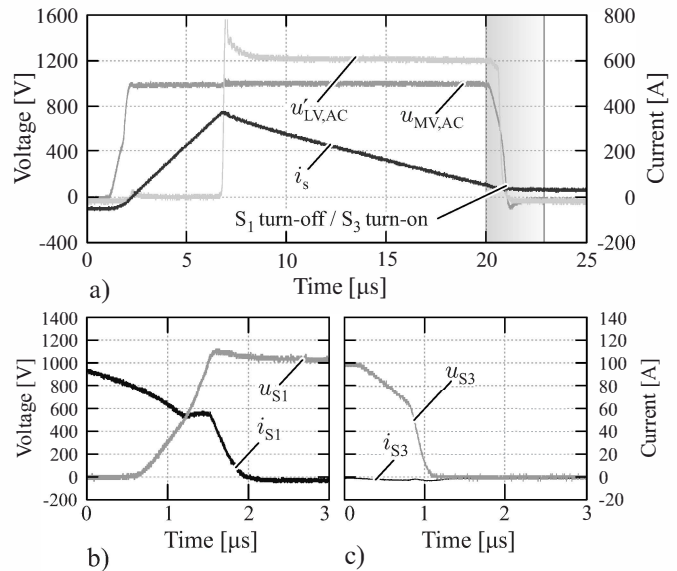


Figure 9: Main waveforms in ZVS with TCM DAB and power from MV side to LV side: a) AC-link waveforms for half switching period; b) Voltage and current in S_1 during the time instant highlighted in a); c) Voltage and current in S_3 during the time instant highlighted in a).

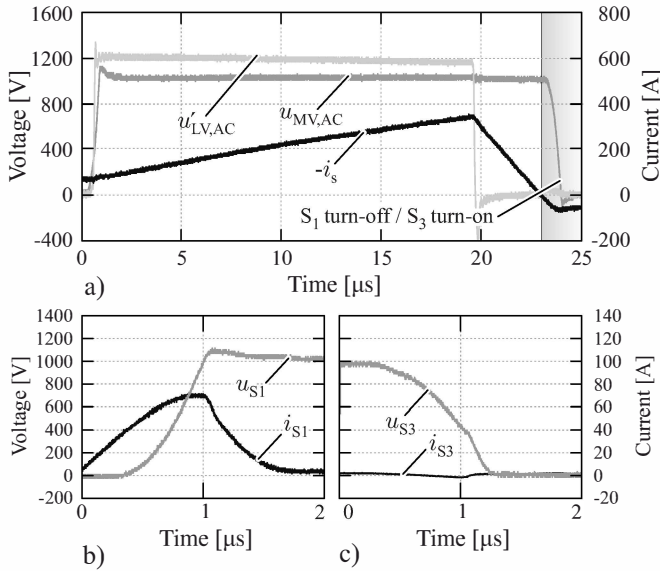


Figure 10: Main waveforms in ZVS with TCM DAB and power from LV side to MV side: a) AC-link waveforms for half switching period; b) Voltage and current in S_1 during the time instant highlighted in a); c) Voltage and current in S_3 during the time instant highlighted in a).

to a negligible value.

In Fig. 10-a) the operation for power from the LV to the MV side is shown with a modification in the modulation scheme which allows the antiparallel diode of S_1 to conduct in the reverse direction by keeping the gate signals of its respective switch on until the reverse recovery charge has been evacuated. The results of this modification in the switching performance of S_1 and S_3 are shown in Figs. 10-b) and c) respectively. As previously explained, the current is allowed to reverse its direction in S_1 before it is turned off, thus its voltage is increased by the switched current and not by the turn-on process of switch S_3 . Therefore the turn-on losses in S_3 are reduced considerably as shown in Fig. 10-c).

Taking all switching processes into account, the switching losses in all switches and diodes of the MV side bridge were measured under ZVS operation for different switched currents, at 25 °C and 120 °C and for power in both directions. In Fig. 11-a), the results for power transfer from MV to LV side are presented. Here, an optimum can be found around 40 A of switched current for operation at 120 °C, reaching a reduction of 40% in the total switching losses. Above this current value, no further reduction on the turn-on losses are achieved whereas the turn-off losses are increased, consequently the overall switching losses are increased.

The results for power flow from LV to MV are shown in Fig. 11-b). It can be seen that the switching losses have an optimum value around 70 A for operation at 120 °C, where a 48% reduction with respect to operation in ZCS is achieved. It can be seen that if higher currents are switched-off, no further reduction of turn-on losses are achieved whereas the turn-off losses are increased.

C. The Saturable Inductor

By inserting a saturable inductor L_{sat} (cf. Fig. 6) in series to the series inductor L_s , the current through the transformer, and consequently through the switches, can be shaped conveniently in order to stay in a low value for a considerable portion of the switching period right before the devices are taken to blocking state. This extra time enables a higher internal carrier recombination in these switches, thus lower charges are removed when the voltage is re-applied to the device, reaching lower ZCS losses. This new

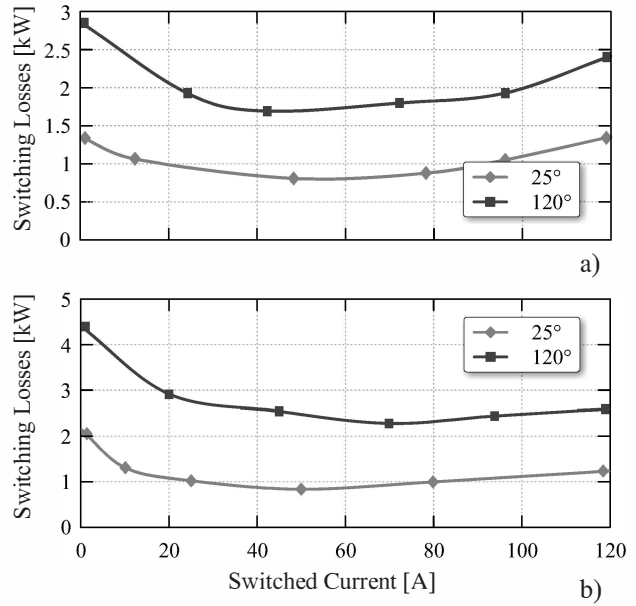


Figure 11: Optimal switched current for switching loss minimization: a) Power from MV to LV side; b) Power from LV to MV side.

current shape can be merged with the previously introduced ZVS modulation, thus combining the features of long recombination time and ZVS.

In this case, a saturable inductor with a saturation current of 35 A was used. While keeping this saturation current constant, the inductance value was modified, whereby three different values were tested: 40 μH , 70 μH and 100 μH . The resulting current waveform for power from the MV side to the LV side, i.e. IGBTs conducting the current, are shown in Fig. 12 for a saturable inductor value of $L_{sat} = 100 \mu\text{H}$. As can be seen from Fig. 12-a), the saturable inductor introduces a time interval before the bridge is taken to freewheeling when the current is comparatively low, thus allowing S_1 and S_2 to recombine a large amount of the charge generated

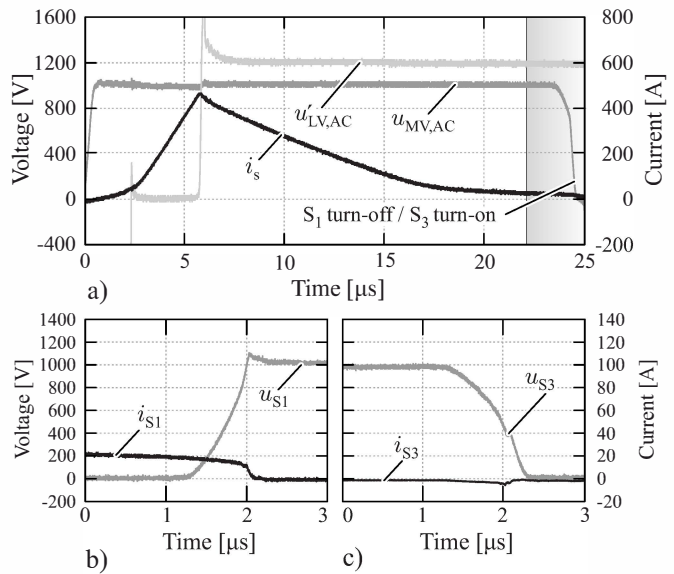


Figure 12: Main waveforms TCM DAB with 100 μH saturable inductor and power from MV side to LV side: a) AC-link waveforms for half switching period; b) Voltage and current in S_1 during the time instant highlighted in a); c) Voltage and current in S_3 during the time instant highlighted in a).

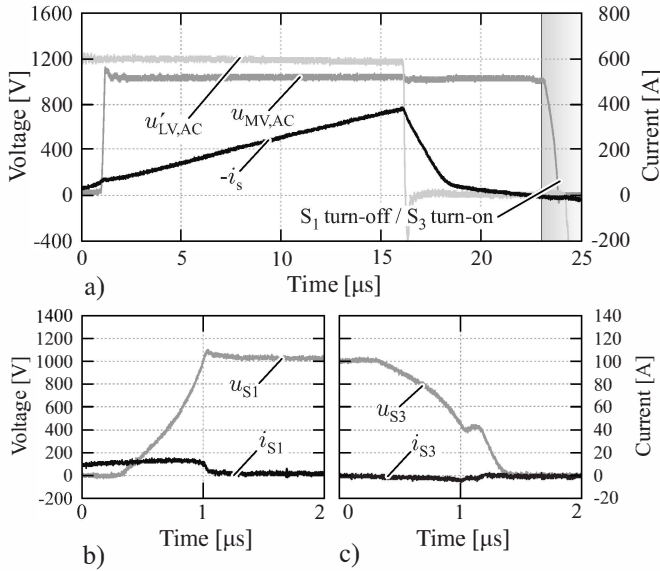


Figure 13: Main waveforms TCM DAB with 100 μH saturable inductor and power from LV side to MV side: a) AC-link waveforms for half switching period; b) Voltage and current in S_1 during the time instant highlighted in a); c) Voltage and current in S_3 during the time instant highlighted in a).

during the conduction phase. In addition, a certain amount of current is turned-off by S_1 (cf. Fig. 12-b)), thus ZVS is achieved in S_3 as shown in Fig. 12-c) and described in the previous section.

The waveforms for power from the LV to the MV side and a saturable inductor $L_{\text{sat}} = 100 \mu\text{H}$ are shown in Fig. 13-a) whereby the diodes in the MV side bridge benefit from the additional time for recombination. In order to achieve soft switching, the current is allowed to reverse its direction through the antiparallel diode of S_1 by keeping this last device turned on until the reverse recovery current has been reached, as can be seen in Fig. 13-b), thus achieving ZVS in S_3 (cf. Fig. 13-c)).

It should be noted that the addition of the saturable inductor L_{sat} to the circuit introduces time intervals, as long as this inductor is not saturated, when considerably low power is transferred from the MV to the LV side. Since the required power to be transferred remains constant, this results in an increased peak current through the circuit, thus higher conduction and switching losses in the LV side. To reduce the impact of the saturable inductor inclusion, the voltages in the MV and LV side are conveniently modified with respect to the traditional modulation in order to rapidly bring the saturable inductor to saturation at the beginning of the half switching period. This can be seen in Fig. 12-a) before $t = 2.5 \mu\text{s}$, when the full difference between $u'_{LV,AC}$ and $u_{MV,AC}$ is applied to the inductors. The result is a moderate increase in the peak current through the circuit resulting in moderate increase in conduction and switching losses, as will be quantitatively analyzed in Section IV-E.

The aforementioned tests were performed for the three values of saturable inductor, 120 $^\circ\text{C}$ and 25 $^\circ\text{C}$ junction temperature and power in both directions. The results for these tests are analyzed and compared with the standard ZCS and the analyzed ZVS modulations in the next section.

D. Switching Loss Reduction Summary

A summary of the previously described switching loss reduction strategies is provided in Fig. 14 for power in both directions and at 25 $^\circ\text{C}$ and 120 $^\circ\text{C}$ junction temperature. As can be seen, a considerable loss reduction can be achieved by combining ZVS

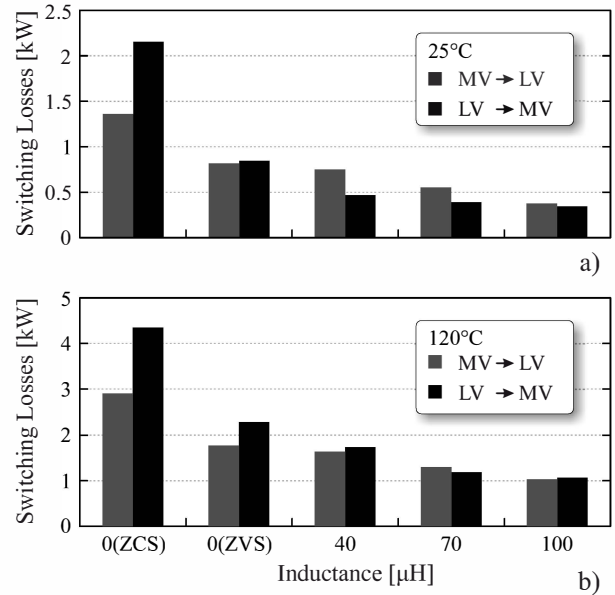


Figure 14: Summary of reduction in switching losses in MV switches with the presented soft switching strategies: a) Junction temperature of 25 $^\circ\text{C}$; b) Junction temperature of 120 $^\circ\text{C}$

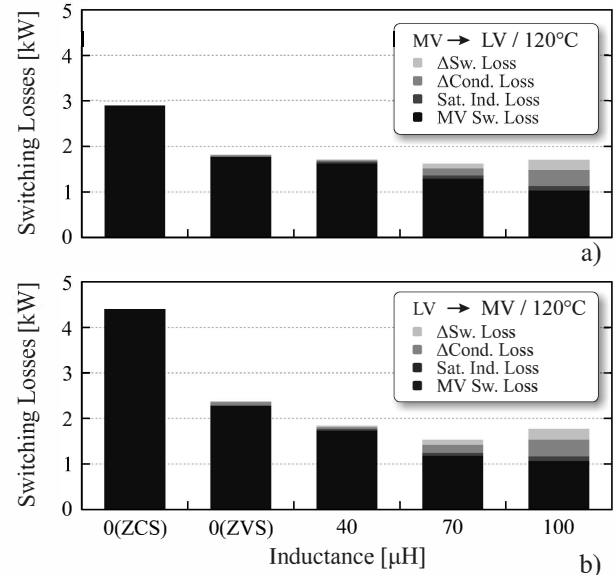


Figure 15: Impact of modified current waveforms on converter performance for junction temperature of 120 $^\circ\text{C}$. The losses in the saturable inductor plus the additional conduction and LV side switching losses are included: a) Power from MV to LV side; b) Power from LV to MV side.

techniques together with the saturable inductor. In the best case, with a 100 μH saturable inductor, the switching losses are more than four times lower for operation at 25 $^\circ\text{C}$ and more than three times lower when operating at 120 $^\circ\text{C}$. These results however, must be compared with the increase in conduction and switching losses introduced by the modification of the current through the transformer and the switches. This final topic will be revised in the next section.

E. Impact on Converter Performance

As previously mentioned, the introduction of the saturable inductor to shape the current through the switches increases the conduction losses in the whole converter and switching losses in

the LV side. Moreover, the saturable inductor generates by itself additional losses which should be added to the total converter losses. In Fig. 15, the aforementioned additional losses are added to the switching losses of the MV side switches obtained from Section IV for the different strategies (please note that these are the additional conduction and switching losses and not the total conduction and switching losses). As can be seen, for power in both directions, the use of a 70 μ H saturable inductor is advantageous with respect to the 100 μ H inductor, as the additional losses introduced by the modified current shape overcome the reduction in switching losses in the MV side in this last case. This means that for this application, the use of a 70 μ H saturable inductor would result the lowest losses in the overall converter.

V. CONCLUSIONS

Analytical and experimental analyses were performed in order to visualize the behavior of the internal charge dynamics in high voltage semiconductors. From here it can be seen that the switching losses in these devices do not depend on the instantaneous value of the current but on the dynamic characteristics of the switch and the shape of the conducted current. Therefore, provided that information about the dynamic characteristics of the internal charge generation/recombination for these devices would be delivered by the device manufacturer, the soft switching losses could be estimated with higher accuracies. Furthermore, by studying the previously proposed ZCS techniques for resonant converters, the two main strategies that help reduce switching losses in MV MF applications were identified: 1) Shaping of current through the semiconductors to allow a high internal carrier recombination in device before the blocking voltage is re-applied and 2) Achievement of ZVS in the turn-on events. These two techniques were implemented in a TCM DAB. By achieving ZVS in the turning-on events, a reduction of up to 40% at 120 °C junction temperature was achieved. The shaping of current in this converter is achieved by means of a saturable inductor in series to the converter's main inductor. With this component, the current was conveniently shaped in order to stay in a low value before the device enters the blocking state, therefore achieving high stored charge recombination.

The combination of these two approaches, ZVS and the saturable inductor, for switching loss reduction resulted in up to four times lower switching losses of the MV side semiconductors with respect to standard ZCS modulation. The impact of the modified current shapes due to the introduction of the saturable inductor on the complete converter resulted in an optimum value for the saturable inductor of 70 μ H which minimizes the overall converter power losses.

REFERENCES

- [1] D. Dujic, F. Kieferndorf, and F. Canales, "Power Electronics Transformer Technology For Traction Applications - An Overview," *PCIM 2011*, 2011.
- [2] C. Zhao and S. Lewdeni-Schmid, "Design, implementation and performance of a modular power electronic transformer (PET) for railway application," *Power Electronics and Applications, European Conference on*, 2011.
- [3] C. Meyer, *Key components for future offshore dc grids*. Shaker, 2007.
- [4] S. Meier, S. Norrga, and H. P. Nee, "New topology for more efficient AC/DC converters for future offshore wind farms," in *4th Nordic Workshop on Power and Industrial Electronics*, 2004.
- [5] P. Monjean, J. Delanoe, J. Auguste, C. Saudemont, J. Sprooten, and Mirzaian, "Topologies Comparison of Multi-Cell Medium-Frequency Transformer for Offshore Farms," in *AC and DC Power Transmission, 2010. ACDC. 9th IET International Conference on*, Mar. 2010.
- [6] L. Heinemann and G. Mauthe, "The universal power electronics based distribution transformer, an unified approach," *Annual Power Electronics Specialists Conference*, pp. 504–509, 2001.
- [7] J. Wang, A. Huang, W. Sung, Y. Liu, and B. Baliga, "Smart grid technologies," *Industrial Electronics Magazine, IEEE*, vol. 3, no. 2, pp. 16–23, 2009.
- [8] H. Reinold and M. Steiner, "Characterization of Semiconductor Losses in Series Resonant DC-DC Converters for High Power Applications using Transformers with Low Leakage Inductance," in *Power Electronics and Applications, European Conference on*, 1999, pp. 1–10.
- [9] J. Taufiq, "Power electronics technologies for railway vehicles," in *Power Conversion Conference*. IEEE, 2007, pp. 1388–1393.
- [10] M. Steiner and H. Reinold, "Medium frequency topology in railway applications," in *Power Electronics and Applications, European Conference on*. IEEE, 2008, pp. 1–10.
- [11] H. Hoffmann and B. Piepenbreier, "High voltage IGBTs and medium frequency transformer in DC-DC converters for railway applications," in *Power Electronics Electrical Drives Automation and Motion (SPEEDAM), International Symposium on*. IEEE, 2010, pp. 744–749.
- [12] D. Dujic, A. Mester, and T. Chaudhuri, "Laboratory scale prototype of a power electronic transformer for traction applications," *Power Electronics and Applications, European Conference on*, vol. i, 2011.
- [13] N. Schibli, "Symmetrical multilevel converters with two quadrant DC-DC feeding," Ph.D. dissertation, EPFL, 2000.
- [14] F. Krismer and J. Biela, "A comparative evaluation of isolated bidirectional DC/DC converters with wide input and output voltage range," *Industry Applications Conference*, vol. 1, no. c, pp. 599–606, 2005.
- [15] G. Ortiz, J. Biela, D. Bortis, and J. W. Kolar, "1 Megawatt, 20 kHz, isolated, bidirectional 12kV to 1.2 kV DC-DC converter for renewable energy applications," in *IPEC 2010*. IEEE, 2010, pp. 3212–3219.
- [16] P. Renstad and H. P. Nee, "On Dynamic Effects Influencing IGBT Losses in Soft-Switching Converters," *IEEE Transactions on Power Electronics*, vol. 26, no. 1, pp. 260–271, 2010.
- [17] A. Elasser and V. Parthasarathy, "A study of the internal device dynamics of punch-through and nonpunch-through IGBTs under zero-current switching," *Power Electronics, IEEE Transactions on*, vol. 12, no. 1, pp. 21–35, 1997.
- [18] L. Lindenm, R. Alvarez, P. Kleinichen, and S. Bernet, "Characterization of a 6 . 5 kV / 500 A IGBT Module in a Series Resonant Converter," in *2011 IEEE Conversion Congress & Exposition*, Phoenix AZ, 2011, pp. 4138–4143.